Spin-Flip Probability in the Inelastic Scattering of 7.48-MeV Neutrons from the 4.43-MeV State of $^{12}C^{\dagger}$

F. D. McDaniel,* M. W. McDonald,‡ M. F. Steuer, and R. M. Wood
University of Georgia, Athens, Georgia 30601
(Received 6 March 1972)

An $(n, n'\gamma)$ coincidence method was used to determine the neutron spin-flip probability in inelastic scattering. The experimental method consists of neutron time-of-flight and neutron-γ coincidence techniques with the deexcitation γ ray detected perpendicular to the neutron scattering plane. The angular distribution of the spin-flip probability for the first $J^{\pi}=2^{+}$ excitation in carbon has been determined at an energy of 7.48 MeV. The neutron spin-flip results were found to be similar to the proton spin-flip results in this energy region. The experimental results were compared to the predictions of an antisymmetrized distorted-wave calculation which did not provide good fits to the spin-flip data. The spin-flip predictions were sensitive to the optical-model parameters and were dominated by spin-orbit distortion in the elastic channels. The mechanism of core polarization dominated the inelastic amplitudes, masking the effects of the effective interaction on the extracore nucleons.

I. INTRODUCTION

The study of spin-dependent forces in the inelastic scattering of nucleons by nuclei has been made difficult because of the insensitivity of the measured angular distributions to these forces. To obtain data more sensitive to the spin-dependent interaction many experimenters have made measurements of the spin-flip probability for proton inelastic scattering.[1-7] These experiments have been possible in part because of the availability of high-resolution proton spectrometers which provide good separation of the excited states of interest. There have been few measurements of the neutron spin-flip probability[8,9] because of the experimental difficulties involved. These measurements have not been made with the high degree of resolution exhibited in the proton experiments.

A method for determining the spin-flip probability in neutron inelastic scattering with a time resolution of less than 3 nsec was described in an earlier report from this laboratory.[10] In the present paper an improved high-resolution method is described. The method employs time-of-flight techniques and involves measuring the correlation between the inelastically scattered neutron and the deexcitation γ which is emitted normal to the reaction plane. This $(n, n'\gamma)$ method is similar to the $(p, p'\gamma)$ method described by Schmidt *et al.*[1] The out-of-plane correlation identifies scattering from the $M=\pm1$ substates of the $J^{\pi}=2^{+}$ state. By applying a theorem due to Bohr[11] it may be shown that scattering from the $M=\pm1$ substates can occur only for nucleons which flip their spins in the scattering process.

The present paper presents the spin-flip results obtained for 7.48-MeV incident neutrons scattered from the first excited state (4.43 MeV) of ^{12}C. Preliminary results have been presented earlier.[12]

II. EXPERIMENTAL APPARATUS AND TECHNIQUES

A. Neutron Source

Neutrons of 7.48-MeV mean energy were produced in a deuterium gas cell bombarded with 4.45-MeV deuterons from the University of Georgia 5-MV Van de Graaff accelerator. The target assembly consisted of a collimator, a suppressor, and a cylindrical gas cell 1.9 cm long. The cell walls were lined with tantalum, and a tantalum disc served as a beam stop. Another tantalum disc with a 0.476-cm-diameter hole was located at the entrance to the gas cell and served as a support for a 2.54×10^{-4}-cm Havar foil. The gas pressure in the cell was 1.95 atm. The collimator ensured that the beam passed into the cell, and the suppressor provided for accurate charge collection. The deuteron energy loss in the foil was 170 keV. The target gas was 120 keV thick for the incident deuterons.

The accelerator beam was pulsed and bunched in the terminal at a 0.5-MHz rate. The beam pulses at the target were less than 1.5 nsec full width at half maximum (FWHM) and provided an over-all time resolution of less than 3 nsec FWHM for the experiment.

B. Scatterer, Detectors, and Shielding

The experimental apparatus is shown in Fig. 1. The scatterer was a sample of naturally occurring

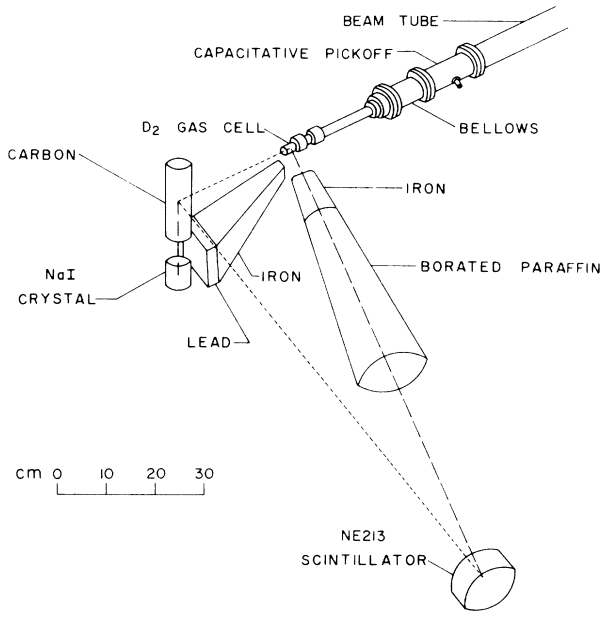

FIG. 1. Experimental apparatus consisting of carbon scatterer, detectors, and shielding. The dashed line represents the flight path of the neutrons scattered elastically and inelastically from the carbon scatterer. The broken line denotes the flight path of the direct neutrons from the gas cell. The path of the deexcitation γ rays is shown as the dot-dash line.

carbon (98.89% ^{12}C) in the form of a graphite cylinder 5.04 cm in diameter and 15.33 cm long. This large sample was chosen to compensate for the low detection efficiency of the apparatus for spin-flip events. The center-to-center distance from the gas cell to the carbon scatterer was 24.7 cm. The large size of the scatterer introduced relatively large multiple-scattering effects and also contributed to the energy width of the neutrons. The maximum neutron energy width due to scatterer size and gas-target thickness was 300 keV. The diameter of the carbon scatterer was approximately one mean free path for the incident neutrons.

The neutron detector, which was chosen because of its neutron-γ pulse-shape discrimination and fast timing capabilities, was an NE213 scintillator 12.7 cm in diameter and 5.08 cm thick. The detector was mounted so that it could be rotated in the reaction plane about the vertical axis of the carbon scatterer. The flight path was maintained at 1 m.

The flux of direct neutrons from the gas target to the neutron detector was attenuated approximately 75% by a shield consisting of iron and borated paraffin. The iron shield was the frustrum of a right circular cone 20 cm long with a mass of 5.7 kg. The borated paraffin shield was the frustrum of a right circular cone 32 cm long with a mass

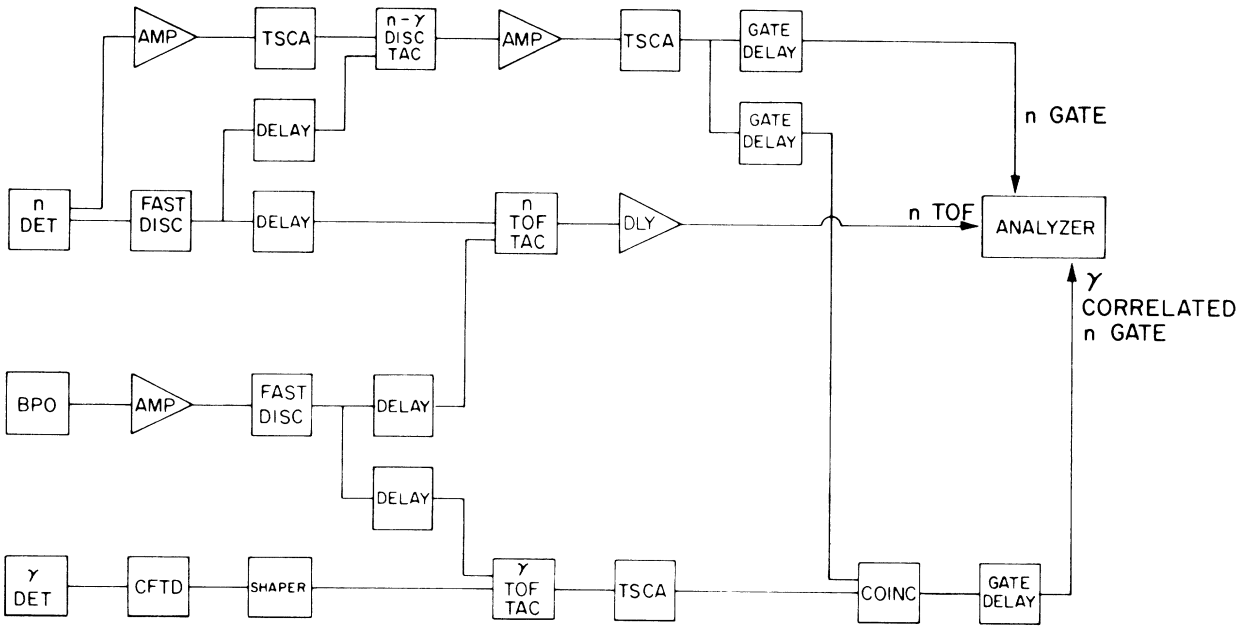

BPO = Beam-pickoff unit
CFTD = Constant-fraction timing discriminator
TSCA = Timing single-channel analyzer

FIG. 2. Block diagram of the time-of-flight electronics.

of 3.6 kg. This shield was made by mixing equal weights of boric acid granules and hot paraffin.

C. Electronics

A block diagram of the electronic components used in this experiment is shown in Fig. 2. The function of the electronics processing the signals from the neutron detector was to establish a bias, distinguish between neutron and γ events, and generate a neutron time-of-flight spectrum. A fast signal from the γ detector initiated collection of a γ-ray time-of-flight spectrum. A typical spectrum is shown in Fig. 3. Events occurring within a narrow time range in this spectrum served to gate the multichannel analyzer and separate the neutron time-of-flight spectrum into a γ-correlated spectrum and a non-γ-correlated spectrum. Neutrons which experienced a spin-flip in inelastic scattering were contained in the γ-correlated spectrum.

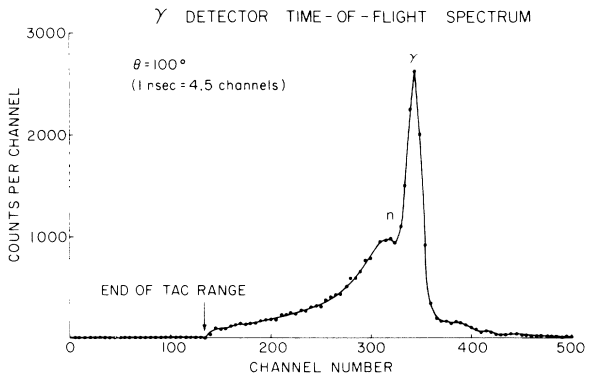

FIG. 3. γ-ray detector time-of-flight spectrum. Increasing time is to the left. The peaks labeled γ and n represent 4.43-MeV γ-ray events and elastically scattered neutron events, respectively. The long tail associated with the neutron peak is produced by multiple-scattering effects and by different flight times for neutrons scattered from the extremities of the sample. A time window was positioned across the γ-ray peak.

D. Accumulation of Experimental Data

Neutron time-of-flight spectra were obtained at 10° intervals for neutron detector angles between 30° and 150° in the laboratory system. γ-correlated and non-γ-correlated spectra were obtained and stored in separate sections of a Nuclear Data 4096 channel analyzer. The time required for data collection at each angle ranged from 6 to 24 h. At each angle alternate scatterer-in and scatterer-out runs, each of duration less than one hour, were were made for equal amounts of charge collected at the target.

A typical set of data is shown in Fig. 4. The elastic and inelastic (4.43-MeV) groups are well resolved in the subtracted spectra except for the low-energy tails which were caused by multiple scattering in the large carbon sample. The background was typically 60–70% of the foreground for the non-γ-correlated spectra and 30% for the γ-correlated spectra. Contributions to the spectra from target contaminants were minimized by periodically cleaning the gas target and collimator assembly and by changing the entrance foil. The

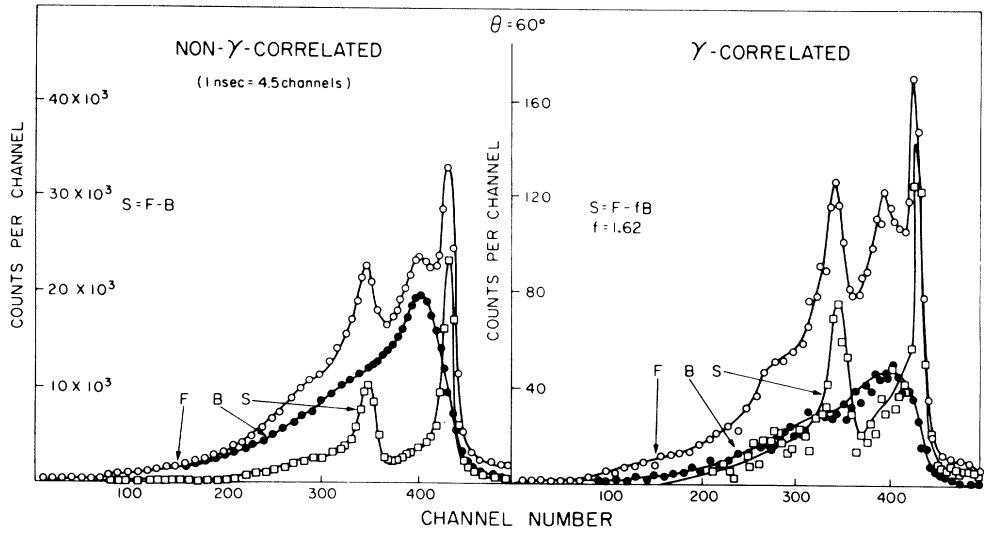

FIG. 4. Typical neutron time-of-flight spectra. Increasing time is to the left in each spectrum. F, B, and S denote foreground, background, and subtracted spectra, respectively. The factor f is defined in the text. The tails to the left of the time-of-flight peaks represent multiple-scattered neutron events. The peak resolution obtained in the subtracted time-of-flight spectra was typically 3 nsec (FWHM).

target cell was evacuated during the experiment and data were collected to measure the effects of target contamination. The gas-out contributions were found to be less than 1% of the subtracted spectra.

III. DATA ANALYSIS AND RESULTS

A. Corrections to Time-of-Flight Spectra

A correction to the time-of-flight spectra was necessary because of a change in the density of the atoms in the target gas due to a local heating of the gas by the incident beam. The correction, which has been discussed by Coon,[13] amounted to <1% in this work.

Other corrections were made for dead-time counting losses in the timing circuits and the multichannel analyzer. All of these corrections were made before the data were reduced further.

B. Separation of Elastic and Inelastic Groups

The elastic and inelastic neutron time-of-flight groups, as seen in the subtracted spectrum of Fig. 4, were not completely resolved because of low-energy tails in the time-of-flight spectra. Calculations verified that the events located in the tails were neutrons multiple-scattered in the carbon sample.

A distinction was made between the multiple-scattered neutrons located in the tails of the time-of-flight peaks and the neutrons multiple-scattered away from the neutron detector. The low-energy tails following the time-of-flight peaks were produced primarily by neutrons that were scattered at some original (θ, ϕ) not necessarily toward the neutron detector and then because of multiple scattering were scattered into the neutron detector. These events will be labeled multiple scattering of the first kind. The second type of multiple scattering consisted of neutrons scattered originally in the direction of the neutron detector and then, because of multiple scattering, were scattered away from the neutron detector, and hence did not appear in the time-of-flight spectrum. These events will be labeled multiple scattering of the second kind. The tails were included in the determination of elastic and inelastic yields and corrections were made for both kinds of multiple scattering.

The spin-flip probability is independent of multiple scattering of the second kind because it is a ratio of the γ-correlated events to the total number of events. The spin-flip probability is not independent of multiple scattering of the first kind because these neutrons were originally inelastically scattered at some (θ, ϕ) such that the $L=2$, $M=\pm 1$ quadrupole radiation had a much smaller probability of being detected by the γ-ray detector. For this reason, multiple-scattered events in the tails of the time-of-flight peaks were not included in the computation of the spin-flip probability.

The first step in extracting yields from a spectrum was to establish the flat background level based on the regions to the left of the inelastic peak and to the right of the elastic peak. The tail of the elastic peak was then extrapolated linearly down to the flat background level. The contribution to a peak due to its tail was deduced by removing the shielding between the gas target and the detector and looking directly at the neutrons from the $D(d,n)^3He$ reaction. These direct neutrons produced a peak without a tail, and comparison to the elastic and inelastic scattering peaks allowed separation of the peaks from their tails.

C. Calculation of the Spin-Flip Probability

The spin-flip probability computation was begun by subtracting the integrated peak areas in the background spectra from the integrated peak areas in the foreground spectra. For the non-γ-correlated events,

$$I1 = I1F - I1B \tag{1a}$$

and

$$E1 = E1F - E1B. \tag{1b}$$

$I1$ and $E1$ are the numbers of counts in the subtracted non-γ-correlated inelastic and elastic peaks, respectively. The γ-correlated background was multiplied by a count-rate correction factor f before subtraction from the γ-correlated foreground. Thus

$$I2 = I2F - f \cdot I2B \tag{2a}$$

and

$$E2 = E2F - f \cdot E2B, \tag{2b}$$

where

$$f = \frac{R_{nF}}{R_{nB}} \frac{R_{\gamma F}}{R_{\gamma B}}. \tag{3}$$

R_n and R_γ are the neutron and γ count rates at the input of the coincidence circuit which identifies the γ-correlated events. The foreground and background rates are identified by F and B, respectively.

An additional correction to the γ-correlated spectrum was made because of scatterer-associated accidental events. For example, a neutron could have been scattered inelastically into the neutron detector, while a γ ray produced by an unrelated event could have been detected in the γ-ray detector. The yield under the apparently γ-corre-

lated elastic peak was used to estimate the number of accidentals under the γ-correlated inelastic peak following a method proposed by Schmidt *et al.*[1] The yield under the apparently γ-correlated elastic peak consists of 100% accidentals. The number of accidentals in $I2$ should be in the same ratio to the total number of inelastic events as the number of accidentals in $E2$ is to the total number of elastic events:

$$\frac{I2A}{I1+I2}=\frac{E2}{E1+E2}. \tag{4}$$

Hence, the number of accidentals in $I2$ may be written

$$I2A=\frac{E2}{E1+E2}\,(I1+I2). \tag{5}$$

The spin-flip probability can then be defined as

$$S(\theta)=\frac{(I2-I2A)/\epsilon_\gamma}{I1+I2},$$

where ϵ_γ is the total electronic efficiency of the γ-ray detector. The efficiency for $L=2$, $M=\pm1$ quadrupole radiation was calculated to be $\epsilon_\gamma = 0.0089 \pm 0.0009$. The details of this calculation are given in the Appendix.

The finite size of the scatterer and γ detector made necessary a final correction to the spin-flip probability because inelastically scattered neutron events could be routed into the γ-correlated spectrum by γ radiation from the $M=0,\pm2$ substates of the $J^\pi = 2^+$ excited state of ^{12}C. This correction was made to the experimentally determined spin-flip probability according to a prescription given by Kolasinski *et al.*[3,14] in which equal populations of the $M=0,\pm2$ substates were assumed. The correction reduced the spin-flip probability at all angles. The reduction was <4% at the angles where the spin-flip probability was 15% or less and <1% at the angles where the spin-flip experienced its maximum values of 30–40%. This is physically what one would expect, since if the spin-flip probability is small the contributions from the other substates ($M=0,\pm2$) will be relatively larger.

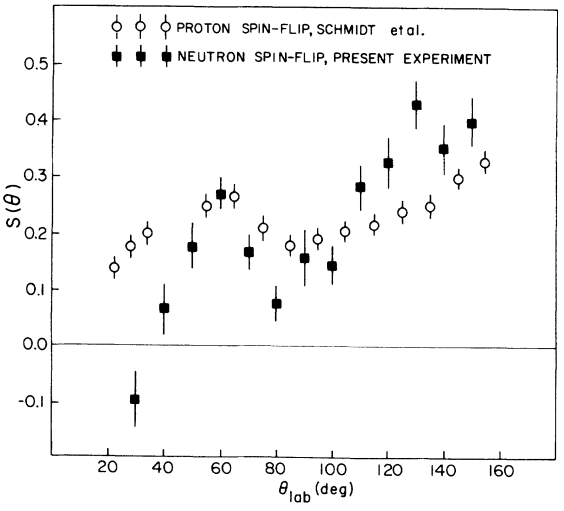

FIG. 5. Angular distributions of the spin-flip probability for ^{12}C. The solid squares represent the spin-flip probability for 7.48-MeV neutrons, while the open circles represent the proton spin-flip results of Schmidt *et al*. (Ref. 1).

The corrected angular distribution of the spin-flip probability is shown in Fig. 5. The error bars on the data are purely statistical counting errors. The negative value of the spin-flip probability at 30° is not physically possible. This error was attributed to inadequate resolution of the elastic and inelastic time-of-flight groups at forward angles. The angle of 30° was the worst case.

The spin-flip probability angular distribution is similar in shape to that found by Schmidt *et al.*[1] for 10–10.5-MeV protons on ^{12}C. These proton energies are similar to the neutron energy in this experiment when the Coulomb barrier is considered. The spin-flip probability results of Schmidt *et al.*[1] show a characteristic backward rise for all energies for which data were taken. This backward rise is also evident in the neutron spin-flip probability for ^{12}C. To illustrate the similarity, the proton spin-flip results of Schmidt *et al.*[1] for an incident proton energy of 10.07 MeV are also shown in Fig. 5. No quantitative conclusions can be drawn from the comparison because of the known energy dependence of the proton spin-flip probability.

D. Relative Elastic and Inelastic Yields Corrected for Multiple Scattering

The angular distributions of the relative elastic and inelastic experimental yields uncorrected for multiple scattering are shown in Fig. 6. The multiple-scattering correction used in this work for the elastic scattering data has been described by Cox[15] and is a combination of analytical and Monte Carlo methods. The fractions of neutrons scattered once, twice, and three or more times were determined by Cox using a Monte Carlo random walk technique. These fractional intensities were related to the dimensions and the total macroscopic cross section of the carbon scatterer. The variation of the cross section with energy was included analytically. The angular distributions of the neutrons scattered once, twice, and three or more times were calculated by an analytical method. The contributions of first-, second-, and third- and higher-order scattering to the experi-

mentally measured angular distribution were found to be 68.2, 21.0, and 10.8%, respectively.

The elastic yield corrected for multiple scattering and flux attenuation was numerically integrated and normalized to the total elastic cross section of 1304 mb reported by Perey and Kinney[16] at 7.54 MeV. The elastic scattering cross section in mb/sr is compared to the 7.54-MeV data of Perey and Kinney[16] in Fig. 7.

The corrected inelastic yield was normalized to mb/sr using the same conversion factor found for the elastic normalization. An analytical correction for multiple scattering and flux attenuation was applied to the cross section for inelastic scattering. This purely analytical correction for the inelastic scattering from cylindrical targets has been described by Engelbrecht[17] and assumes isotropy of the inelastic angular distribution. Its calculation depends on both the dimensions and the total macroscopic cross section of the scatterer. Energy variations of the cross sections were included analytically. Figure 8 shows the uncorrected and corrected results as well as the 7.54-MeV data of Perey and Kinney.[16] The multiple scattering and flux attenuation correction increased the value of the cross section at each point by approximately 20%.

IV. THEORETICAL ANALYSIS

A. Introduction

Many of the reported spin-flip probability measurements have been analyzed in the distorted-wave Born approximation (DWBA) using either a collective model or a model which employs both core polarization and a microscopic treatment of the extracore nucleons. The DWBA is not strictly applicable to ^{12}C, but some investigators have applied the approximation to the analysis of ^{12}C data with some degree of success. In the present work the problem of analysis is further complicated because of the uncertainty in the relative importance of direct interaction processes as compared to the formation of a compound nucleus. At the mean incident neutron energy of 7.48 MeV there is resonance behavior in the total neutron cross section. This energy region has been examined by Davis and Noda[18] with an energy resolution of 25 keV. Their results indicate that in the region 7.48 $\pm$ 0.150 MeV the cross section is nearly constant, indicating that no single level is dominating the cross section. In the present work a DWBA analysis was performed with the expectation that some of the general features of the experimental data could be reproduced by the calculation. An estimate of the validity of the calculation is given in Sec. V. This study of 7.48-MeV neutrons on ^{12}C was made preliminary to further studies with 16–20-MeV neutrons on ^{12}C, ^{28}Si, ^{32}S, and ^{40}A, where the direct interaction mechanism may be expected to dominate the scattering.

At energies where the direct interaction theories may be expected to apply the DWBA methods have

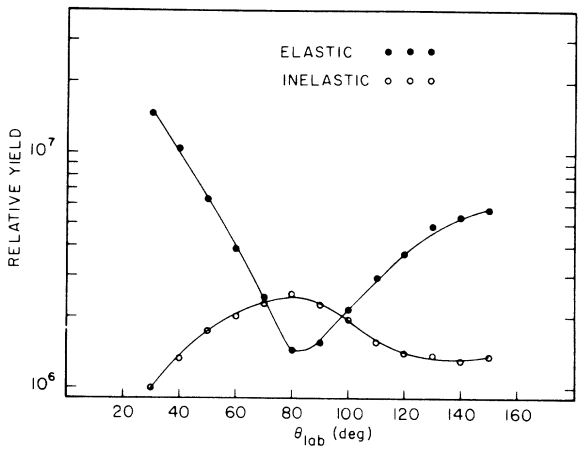

FIG. 6. Angular distributions of the relative elastic and inelastic experimental yields. The statistical counting errors are smaller than the size of the data points.

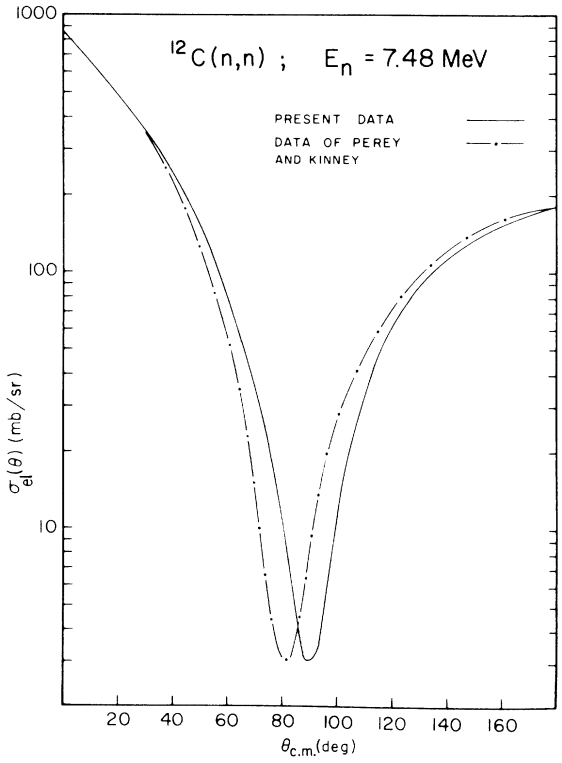

FIG. 7. Elastic differential cross section in mb/sr. The angular distribution of elastic scattering is compared with the 7.54-MeV data of Perey and Kinney (Ref. 16).

had some success in describing the inelastic scattering of protons from several different nuclei.[2-6] The extended-optical-model or collective-model approach has had considerable success in predicting the differential cross sections but only a limited success in predicting spin-flip probabilities. The microscopic approach including core polarization has also had little success in predicting spin-flip probabilities. These results are assumed to be a consequence primarily of inadequate knowledge of the nuclear spectroscopy of the target nucleus and uncertainty as to the character of the nuclear-reaction mechanism. In addition, these calculations have generally excluded exchange effects, which have been found[19] to be very important. At lower energies the compound-nucleus mechanism has been shown[7] to dominate the reaction. The extent of compound-nucleus effects in the present work is difficult to estimate. No attempt was made to include these effects in the calculations.

The measurements of the inelastic differential cross section and spin-flip probability were analyzed using the code MEPHISTO, which has been described in detail by Geramb and Amos.[20] This direct reaction calculation employs a transition operator which includes a microscopic two-nucleon component with exchange effects and a macroscopic core polarization component.[21] The core polarization interaction component indirectly allows for interactions between the projectile and the remaining target nucleons by means of virtual excitations of the core nucleons.

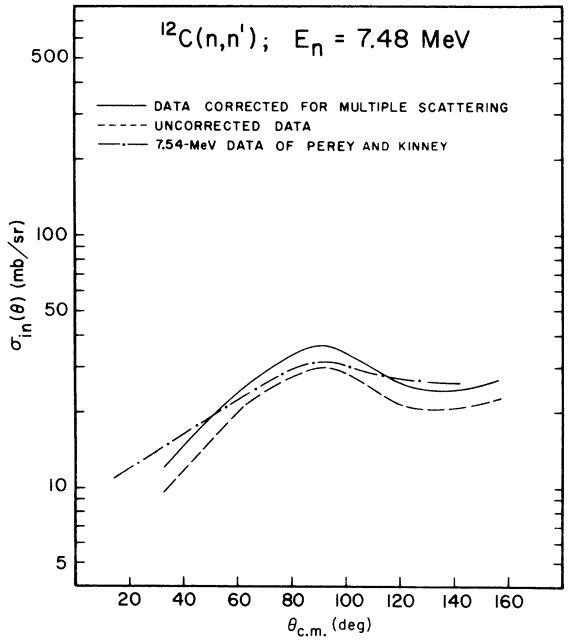

FIG. 8. Inelastic differential cross sections in mb/sr. The angular distribution, corrected and uncorrected for multiple scattering, is compared with the 7.54-MeV results obtained by Perey and Kinney (Ref. 16).

The inelastic differential cross section and the spin-flip probability are determined from the calculated partial cross section σ_{if}, where i and f denote the initial- and final-state spin projections of the incident nucleon with the axis of quantization normal to the scattering plane. Thus

$$\frac{d\sigma}{d\Omega} = (\sigma_{++} + \sigma_{-+} + \sigma_{+-} + \sigma_{--}),$$

$$S(\Omega) = \frac{\sigma_{-+} + \sigma_{+-}}{d\sigma/d\Omega}.$$

The partial cross sections σ_{-+} and σ_{+-} can receive contributions from (1) spin-flip induced by spin-orbit effects in the optical-model potential in both the initial and final elastic scattering states,[22] and from (2) spin-flip induced by the nucleon-nucleon interaction.

B. Parameter Specification

The distorted-wave functions describing the elastic scattering states are solutions of Schrödinger's equation for the optical-model potential that best describes the elastic scattering data. The optical-model program JIB3-WS was used to perform an extensive parameter search. The initial set of parameters used were those determined by Haglund *et al.*[23] for proton elastic scattering from ^{12}C in the 7–10-MeV region.

Because elastic polarization data were not available, no unique set of parameters was determined. Instead, two sets of parameters were chosen, both of which provided fairly good fits to the elastic scattering angular distribution. The two fits are

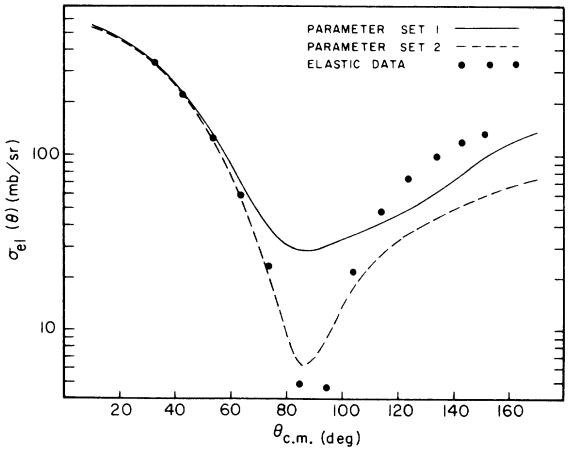

FIG. 9. Optical-model predictions for the elastic differential cross sections. The two sets of parameters are given in Table I.

compared to the experimental data in Fig. 9. The noticeable differences between these two fits will be utilized later in the discussion of the results. The two sets of parameters are given in Table I. The potential strengths are in MeV and the radii and diffuseness parameters are in F.

The core polarization contribution was determined from a collective model representation.[21] The core polarization strength is related to the value of the stiffness parameter, C_L. The core polarization interaction accounts for the numerous small amplitude configurations that are missing because of an incomplete description of the nuclear states. That part of the nucleon-nucleon interaction not ascribed to core polarization was taken to be the long-range part of the Hamada-Johnston potential[24] obtained by truncating at a distance of 1.05 F.

The single-particle bound-state wave functions were chosen to be harmonic-oscillator states. The oscillator frequency, ω_0, was taken to be[25]

$$\hbar\omega_0 \simeq 41A^{-1/3} = 17.9 \text{ MeV}.$$

The target spectroscopy for the $J^\pi = 0^+$ ground state of ^{12}C was assumed to be 100% of a closed $1p_{3/2}$ shell. The first excited state of ^{12}C has been represented in terms of particle-hole states by Gillet and Vinh Mau.[26]

C. Model Shortcomings

(1) The strongly excited 2^+ state in ^{12}C is evidence that the elastic scattering is coupled to the scattering from the first 2^+ state, which makes the DWBA questionable. A semiquantitative estimate of the correctness of DWBA is given in the following section on results.

(2) Compound-nucleus effects were neglected. Justification for this assumption can come only from the results presented in the next section. For example, the forward peaking of the elastic cross section is an indication of a sizable direct interaction contribution.

TABLE I. Optical-model parameters.

Parameters	Set 1	Set 2
V_0	49.6	51.0
r_1	1.117	1.12
a_1	0.3	0.2036
$4W_D$	4.0	4.8
r_3	1.0	1.05
a_3	0.4	0.45
V_{so}	−6.091	−6.35
W_{so}	0.0	0.0
r_4	1.1	1.15
a_4	0.4	0.3

(3) The target spectroscopy which was assumed is incomplete. The particle-hole description of ^{12}C was taken as a first approximation only.

(4) The antisymmetrized DW computer code MEPHISTO of Geramb and Amos[20] allows one to make simplifying assumptions. The two-body interaction used in the model calculations neglected spin-orbit and tensor terms. Also, the core interaction was taken to be spin-independent, and the spin-orbit term in the core was not deformed. These assumptions seemed reasonable in the light of large uncertainties resulting from shortcomings (1) and (3) given above.

V. RESULTS

Using Set 1 of the optical model parameters given in Table I the inelastic differential cross section and the spin-flip probability (2^+ state) were calculated. Two alternative final-state configurations were assumed for the 2^+ state of 4.43 MeV:

$$|2^+\rangle_1 = |(1p_{3/2}^{-1}, 1p_{1/2}), 2^+\rangle,$$

$$|2^+\rangle_2 = 0.91|(1p_{3/2}^{-1}, 1p_{1/2}, 2^+\rangle + 0.3|(1p_{3/2}^{-1}, 1f_{7/2}, 2^+\rangle - 0.29|(1s_{1/2}^{-1}, 1d_{5/2}, 2^+\rangle.$$

The results were very insensitive to the configuration(s) of the excited state. The calculated cross section for the single configuration is shown in Fig. 10, where it is compared to the data. The stiffness parameter C_L was 61 MeV and the core amplitude was about 5 times the effective interaction amplitude. Thus, while the effective interaction contribution to the cross section was only about 4% of the measured cross section, the effect of interference terms in the coherent sum was to fix the core contribution at about 60% of the measured cross section. This large contribution by the core is consistent with the known collective nature of ^{12}C, which is believed to be permanently deformed with $\beta_2 = 0.6$.[27] The value of the stiffness parameter which gives a fit to the cross section may be used to estimate the validity of the DWBA assumption. Using an average interaction strength represented by choosing[21] $\langle k \rangle = 50$ MeV and assuming a $p_{1/2} \rightarrow p_{3/2}$ transition including core polarization, we estimate $\beta_2^{(c)}$, the deformation parameter associated with the core, to be roughly 0.7 for $C_L = 61$ MeV. Thus the core contribution alone is $(\beta_2^{(c)}/\beta_2)^2 \simeq 1.4$ times the cross section predicted by the collective model if β_2 is taken to be 0.6. While this indicates that the DWBA is not valid in detail, it suggests that it may have some general validity. For example, the shape of the differential cross section is reproduced in a general way although the detail in the cross section is not reproduced. The calculated spin-flip probability re-

produced only the most general features of the data. Core polarization effects dominated the calculations, and the number of configurations in the 2^+ state did not have a large effect on the result. This effect persisted even when all seven configurations given by Gillet *et al.*[26] were included.

The results for the calculated spin-flip probability were found to be sensitive to the optical-model parameters. Set 2 of Table I predicted more structure in the spin-flip probability and gave the best fit to the data. The calculation was performed using the second of the configurations given previously for the 2^+ state. The calculated inelastic cross section could not be distinguished from that shown in Fig. 10. The calculated spin-flip probability is compared to the data in Fig. 11. The minimum near 90° and the backward-angle peak near 140° are reproduced in a general way. The predicted forward-angle peak is not seen in the data, and the over-all fit to the data must be called poor. It should be remembered, however, that the errors indicated for the data points are statistical only and do not reflect the probable errors resulting from the method used to separate the elastic and inelastic peaks of the time-of-flight spectra. These errors are believed to be greatest at the forward angles.

VI. CONCLUSION

In the preceding section measurements of the inelastic differential cross section and the spin-flip probability for 7.48-MeV neutrons scattered from the first 2^+ state in ^{12}C have been compared to predictions of a DWBA calculation. All of the theoretical fits to the data were dominated by the core polarization. Thus, although the fits to the inelastic differential cross section were reasonably good, the predictions were found to be not very sensitive to the number of single-particle transitions which were assumed in the calculations. The spin-flip probability predictions were only slightly more dependent on the assumed spectroscopy of the extracore nucleons, but these effects were negligible in comparison to the contributions from the core. It is clear, therefore, that for the simple spectroscopy assumed in this work the Hamada-Johnston contribution to either the differential cross section or the spin-flip probability cannot be used as a sensitive test for the spectroscopy of the nuclear states.

The observation that the predicted spin-flip probability showed a dependence on the choice of optical-model parameters supports the conclusion of Kolata and Galonsky[5] that meaningful information regarding the spin dependence of the reaction mechanism producing the excited state can be obtained from spin-flip measurements only for nuclei having well-defined optical-model parameters. This is a consequence of the large spin-flip contribution produced in the elastic channels by the spin-orbit potential. This elastic scattering spin-flip is the only source of spin-flip for the dominant core polarization amplitudes, since the core polarization was restricted to have no reaction spin-flip component. The simplifying assumptions referred to in Sec. IV C (4) appear to be justified by this result in view of the probable errors of experiment and theory. For heavier nuclei and for higher in-

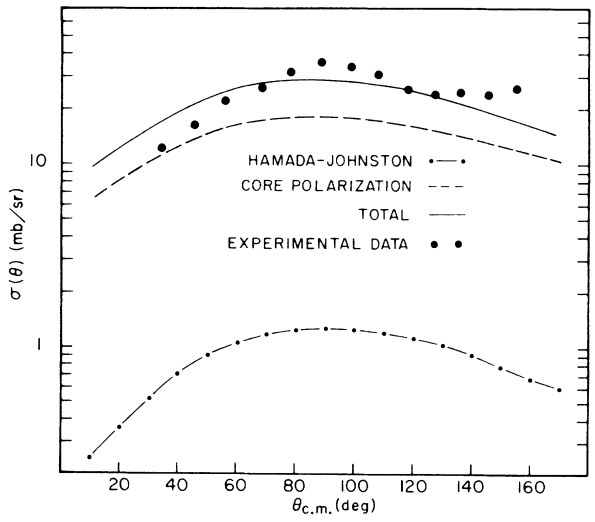

FIG. 10. Predictions of the Hamada-Johnston interaction and core polarization for a single transition are compared to the inelastic differential cross section.

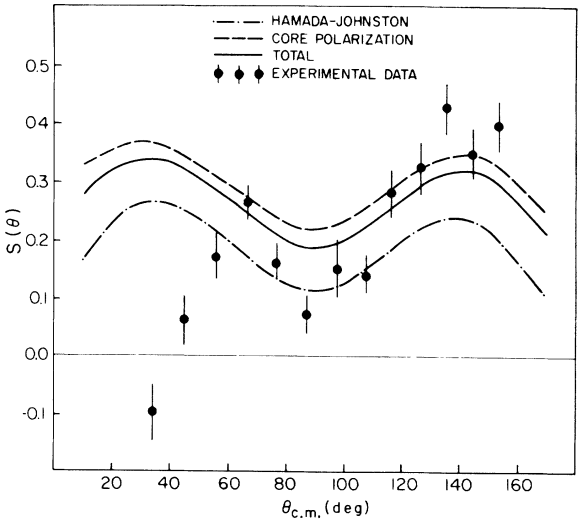

FIG. 11. Predictions of the Hamada-Johnston interaction and core polarization are compared to the spin-flip probability using the optical-model parameters of Set 2 (see Table I).

cident neutron energies, spin-dependent terms in the effective interaction and the core might reasonably be expected to lead to better agreement with the data.

VII. ACKNOWLEDGMENTS

We would like to especially thank Dr. K. A. Amos, formerly of the University of Georgia and presently at the University of Melbourne, Australia, for the use of his DWBA code, MEPHISTO. Also, we want to express our appreciation to Dr. W. G. Love and Dr. L. Owen for many helpful theoretical discussions.

APPENDIX

The energy-dependent efficiency of the neutron detector ϵ_n was calculated using the relation

$$\epsilon_n = (1 - B/E_n)\epsilon_{n0},$$

where ϵ_{n0} is the detection efficiency with zero electronic bias, E_n is the neutron energy, and B is the electronic bias level expressed as a neutron energy. In this work the bias was 0.56 MeV and was set using a radioactive ^{137}Cs source. The efficiency at zero bias was computed according to the method of Elwyn *et al.*[28] The total neutron cross-section data for carbon used in the calculation were taken from Kunz and Schintlmeister.[29] The total neutron cross section for hydrogen was computed using an expression given by Marion and Young.[30]

In the calculation of the γ-detector efficiency ϵ_γ the scatterer was divided into a large number of stacked disc elements and the contribution of each to the efficiency was computed. A description of the computations can be given in terms of the following parameters:

(1) the weighting factor R which is the ratio of the D$(d,n)^3$He cross section averaged over the disc to the value of the cross section averaged over the entire scatterer,

(2) the probability T that a γ ray produced in the disc is transmitted through the scatterer material between the disc and the detector,

(3) the solid angle D subtended at the face of the detector by the scatterer disc,

(4) the fraction F_n of the $M = \pm 1$ substate quadrupole radiation which is emitted into the solid angle subtended by the detector,

(5) the intrinsic detection efficiency ϵ_i of the NaI detector for deexcitation γ radiation, and

(6) the fraction F_B of events in the γ detector which yielded signals above the electronic bias.

The first three factors were used to calculate the effective solid angle of the disc subtended at the detector according to the equation

$$\Omega_{\text{eff}} = RTD .$$

The value of R was determined using a functional representation of the D$(d,n)^3$He cross section given by Dickens and Perey.[31] The value of T was taken to be unity for this work for two reasons. First the mean free path for the γ radiation was comparable to the length of the scatterer. Second, the Compton-scattering cross section was orders of magnitude greater than either the photoelectric or the pair-production cross section for photons of this energy, and the associated scattered radiation was strongly forward peaked. The value of D was determined by using a Monte Carlo code described by Williams[32] in which the solid angle of one disc subtended at the face of the NaI detector was computed.

After the effective solid angle was calculated, the fraction F_n of $M = \pm 1$ quadrupole radiation reaching the detector was determined by integrating the appropriate spherical harmonic over Ω_{eff}. The radiating disc was then approximated by a point source, and the intrinsic efficiency of the detector ϵ_i was computed. Based on estimates in the literature,[33] the error in the point-source approximation was approximately 5% at the bottom of the scatterer and 1% at the top.

The product of F_n and ϵ_{in} is the efficiency for the detection of a γ radiation emitted by a single disc. When averaged over the total number of discs making up the scatterer, the over-all efficiency of the apparatus at zero electronic bias, $\epsilon_{\gamma 0}$, results:

$$\epsilon_{\gamma 0} = \frac{1}{N}\sum_{n=1}^{N} F_n \epsilon_{\text{in}} .$$

The zero-bias efficiency must be multiplied by the fraction of detected events above the electronic bias in order to obtain the total detection efficiency ϵ_γ for the complete experimental system used,

$$\epsilon_\gamma = \epsilon_{\gamma 0} F_B .$$

The value of ϵ_γ which resulted from the computation was 0.0089 ± 0.0009. The effect of the shielding in the vicinity of the detector on ϵ_γ was estimated to be negligible compared to the errors inherent in the calculation.

†Research supported by the National Science Foundation.

*Present address: Department of Physics, University of Kentucky, Lexington, Kentucky 40506.

‡Present address: Department of Physics, Berry College, Mount Berry, Georgia 30149.

[1]F. H. Schmidt, R. E. Brown, J. B. Gerhart, and W. A. Kolasinski, Nucl. Phys. 52, 353 (1964).

[2]D. L. Hendrie, C. Glashausser, J. M. Moss, and J. Thirion, Phys. Rev. 186, 1188 (1969).

[3]W. A. Kolasinski, J. Eenmaa, F. H. Schmidt, H. Sherif, and J. R. Tesmer, Phys. Rev. 180, 1006 (1969).

[4]M. A. Wilson and L. Schecter, Bull. Am. Phys. Soc. 16, 535 (1971).

[5]J. J. Kolata and A. Galonsky, Phys. Rev. 182, 1073 (1969).

[6]S. Kobayashi, S. Motonaga, Y. Chiba, K. Katori, T. Wada, A. Stricker, and T. Fujisawa, J. Phys. Soc. Japan 29, 1 (1970).

[7]D. B. Nichols, R. G. Arns, H. J. Hausman, and R. G. Seyler, Phys. Rev. 183, 945 (1969).

[8]R. C. Braley, M. A. Nagarajan, M. W. Gilpatrick, and R. W. Finlay, Phys. Letters 26B, 248 (1968).

[9]D. Spaargaren and C. C. Jonker, Nucl. Phys. A161, 354 (1971).

[10]M. W. McDonald, F. D. McDaniel, R. M. Wood, and M. F. Steuer, Bull. Am. Phys. Soc. 15, 1329 (1970).

[11]A. Bohr, Nucl. Phys. 10, 486 (1959).

[12]F. D. McDaniel, M. W. McDonald, M. F. Steuer, and R. M. Wood, Bull. Am. Phys. Soc. 16, 1163 (1971).

[13]J. H. Coon, in *Fast Neutron Physics, Part I,* edited by J. B. Marion and J. W. Fowler (Interscience, New York, 1960).

[14]W. A. Kolasinski, Ph.D. dissertation, University of Washington, 1967 (unpublished).

[15]S. A. Cox, Nucl. Instr. Methods 56, 245 (1967).

[16]F. G. Perey and W. E. Kinney, Oak Ridge National Laboratory Report No. ORNL-4441, 1968 (unpublished), p. 30.

[17]C. A. Engelbrecht, Nucl. Instr. Methods 80, 187 (1970).

[18]J. C. Davis and F. T. Noda, Nucl. Phys. A134, 361 (1969).

[19]F. D. McDaniel and K. A. Amos, Nucl. Phys. A180, 497 (1972); K. A. Amos and H. V. Geramb, in *Proceedings of the International Conference on Properties of Nuclear States, Montréal, Canada, 1969,* edited by M. Harvey *et al*. (Presses de l'Université de Montréal, Montréal, Canada, 1969).

[20]H. V. Geramb and K. A. Amos, Nucl. Phys. A163, 337 (1971).

[21]W. G. Love, Nucl. Phys. A127, 129 (1969); W. G. Love and G. R. Satchler, *ibid.* A101, 424 (1967).

[22]G. R. Satchler, Nucl. Phys. 55, 1 (1964).

[23]R. F. Haglund, Jr., C. A. Pearson, G. W. Morrison, and G. W. Westley, Bull. Am. Phys. Soc. 15, 1316 (1970); R. F. Haglund, Jr. (private communication).

[24]T. Hamada and I. D. Johnston, Nucl. Phys. 34, 382 (1962).

[25]A. Bohr and B. R. Mottelson, *Nuclear Structure* (Benjamin, New York, 1969), Vol. 1, p. 209.

[26]V. Gillet and N. Vinh Mau, Nucl. Phys. 54, 321 (1964).

[27]P. H. Stelson and L. Grodzins, Nucl. Data 1A, 21 (1965).

[28]A. Elwyn, J. V. Kane, S. Ofer, and D. H. Wilkinson, Phys. Rev. 116, 1490 (1959).

[29]W. Kunz and J. Schintlmeister, *Nuclear Tables, Part II* (Pergamon, Frankfurt, 1965), Vol. I, pp. 224–227.

[30]J. B. Marion and F. C. Young, *Nuclear Reaction Analysis* (North-Holland, Amsterdam, 1968), pp. 14–19.

[31]J. K. Dickens and F. G. Perey, Nucl. Sci. Eng. 36, 280 (1969).

[32]I. R. Williams, Nucl. Instr. Methods 44, 160 (1966).

[33]C. C. Grosjean and W. Bossaert, *Table of Absolute Gamma-Ray Detection Efficiencies* (Snoeck, Ghent, Belgium, 1965), p. 226.